An Adaptive Airspace Model for Quadcopters in Urban Air Mobility

Quan Shao, Ruoheng Li, Min Dong, and Chengcheng Song

***Abstract*— The emerging usage of quadcopters in Urban Air Mobility has urged airspace design to be precise and dynamic to mitigate collision risks. This paper proposes an adaptive AirMatrix model to obtain the block size of AirMatrix that is calculated through the acceptable track deviation of quadcopters by considering GPS signal quality and wind field. First, the acceptable GPS-induced deviation is calculated to meet the safety tolerance by analyzing the distributions of GPS-induced deviation under different signal quality levels. Second, a dynamic modeling and simulation method is applied to assess the wind impact on the track deviation accurately. The wind-induced deviation is calculated using a wind effect model considering surface friction and turbulence. Results show that the proposed model can reduce airspace conserveness by providing 45 percent available blocks more than the previous model. By considering the wind impact, the adaptive AirMatrix improves the safety performance of blocks at levels ranging from 4.9% to 95.5%, compared with the model without considering wind impact. The adaptive AirMatrix model provides a delicate and targeted approach to design airspace for quadcopters, which benefits traffic management in Urban Air Mobility.**

***Index Terms*— Low-altitude airspace management, UAS traffic management, Urban air mobility.**

I. Introduction

UNMANNED aerial vehicle (UAV) is one of the rising fields in the aviation industry. It has exerted its advantage in civil, commercial, and military fields, playing its full role in agricultural management, environmental research, and emergency rescue [1]. With the development of electric propulsion and sensing system, the realization of Urban Air Mobility (UAM) has become possible [2]. In order to ensure the safety, capacity, and throughput of UAM, UAV traffic management (UTM) has become essential [3].

As one of the most common types of drones applied in UAM, quadcopters have been widely used in operation surveying, surveillance, and logistics due to their simple design, low price, ease-of-use, and flexible movement. However, researchers found that the collision risk among quadcopters has been one of the primary risks associated with UAVs [4] and should be managed intrinsically by rationally designing the airspace [5].

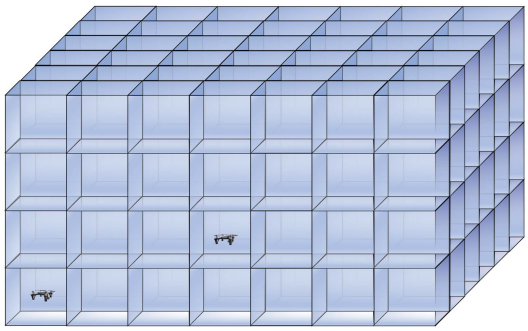

Fig. 1. Conventional AirMatrix model.

The airspace design not only significantly affects the potential risk in UTM, but also yields the optimization of the capacity of airspace *per se* [6]. Generally, airspace models in UTM can be divided into four types, i.e., Full Mix, Layers, Zones, and Tubes [7]. As summarized in Table I, the tube-type airspace can be considered an appropriate model for quadcopter due to its high safety level.

Among the tube-type models, an AirMatrix model has been proposed and widely applied [15]. As illustrated in Fig.1, the airspace is divided into blocks with uniform size. As the centers of blocks are the pre-defined path nodes for quadcopters, the size of blocks should be set to ensure the possibility of tracking deviation of quadcopters within the acceptable level. However, the uniform size of blocks cannot meet the requirement of dynamic risk management based on the concept of Adaptive Urban Airspace management (AdUrAM) [16], which pointed out that urban airspace should be managed dynamically according to traffic demand and associated risks. Specifically, an adaptive design of AirMatrix is essential in mission planning tasks in UAM [18], [19], [20], [21], [22], [23]. Hence, an adaptive and dynamic design of the block size should be considered to manage the potential collision risks among quadcopters.

The block size of AirMatrix is related with the model uncertainty of quadcopters. In the current research, the factor considered in designing the AirMatrix is limited to the uncertainty in the navigation performance of UAVs. For

Manuscript received 13 December 2021; revised 19 April 2022, 23 July 2022, and 12 October 2022; accepted 1 November 2022. Date of publication 10 November 2022; date of current version 8 February 2023. This work was supported in part by the National Basic Research Program of China under Grant 2018YFC0809500, in part by the National Natural Science Foundation of China under Grant 71874081, in part by the Jiangsu Province Natural Science Foundation under Grant BK20201296, and in part by the Innovation Plan Project of Nanjing University of Aeronautics and Astronautics under Grant xcxjh20210704. The Associate Editor for this article was D. Sun. *(Corresponding author: Quan Shao.)*

Quan Shao, Ruoheng Li, and Min Dong the College of Civil Aviation, Nanjing University of Aeronautics and Astronautics, Nanjing 211100, China (e-mail: shaoquan@nuaa.edu.cn; liruoheng@nuaa.edu.cn; mindong@nuaa.edu.cn).

Chengcheng Song is with the College of Civil Engineering, Hunan University, Changsha 410081, China (e-mail: songchengcheng@nuaa.edu.cn).

Digital Object Identifier 10.1109/TITS.2022.3219815

TABLE I
PREVIOUS RESEARCH ON URBAN AIRSPACE STRUCTURE

Concept	Definition	Safety	Capacity	Source
Full Mix	No restrictions on the path of drones. The drones choose a conflict free path by utilizing airborne detection system, like the free-flight concept in civil aviation.	Low	High	[2], [7]-[9]
Layers	Airspace is segmented into vertical bands according to the operation heading range and speed span, like the hemispheric rules in the civil aviation.	Moderate	Moderate	[7], [10]
Zone	The airspace is divided into circular or radial zones, and aircraft can flexibly choose flight altitude.	Moderate	Moderate	[11]-[12]
Tubes	A graph with nodes and edges constructs the conflict free routes.	High	Low	[13]-[23]

instance, Pongsakornsathien et al. [17] proposed an airspace model based on the position dilution of precision (PDOP) of the navigation system. Similarly, Dai et al. [18] proposed an airspace model influenced by the GPS-induced tracking deviation. However, environmental disturbances such as wind can also affect the tracking accuracy of UAVs, which is not considered in previous models. Moreover, the current research did not consider the maneuverability and dynamics of UAVs in designing the AirMatrix, which reduces the reliability of the airspace model [20].

The model uncertainties of quadcopters mainly incorporate parametric and nonparametric uncertainty [24]. The difference between the two centers upon their source and measurement. The former characterizes the inherent system parameters (e.g., time-varying payload [24]), while the latter considers the external disturbances (e.g., wind). The time-varying system parameters usually occur in particular situations, such as in the process of firefighting aircraft unloading water, which is out of the scope of this paper. As the airspace design should adapt to the external environment, this paper focuses on investigating the impact of nonparametric uncertainty.

The effect of nonparametric uncertainty acting on the system can be assessed by two methods. First, the nonparametric uncertainty can be modeled as a bounded space. The system performance under bounded disturbance can be assessed by reachable sets computation based on mixed monotone systems theory [25], [26], [27]. The reachability computation has wide applications in controller design and verification [25], Simplex switching logic design [28], and conflict-free path planning algorithms design [29]. Second, the effect of external disturbances on the quadcopters can also be quantified based on simulation [30], [31], [32], [33]. Tran et al. [30] conducted both experiments and simulations to compare the trajectory of a quadcopter under an actual wind field and the corresponding wind model. The results demonstrate that simulators can accurately predict the motion of quadcopters under

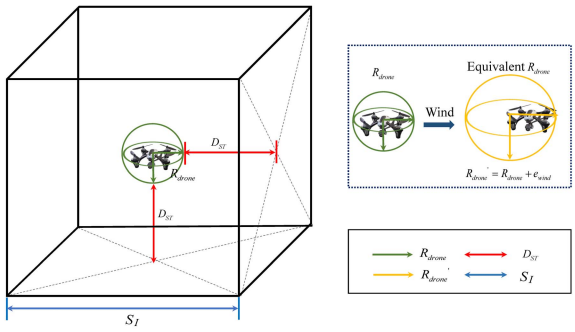

Fig. 2. Illustration of the block in adaptive AirMatrix.

wind disturbances with the wind effect model. Considering the nonlinear characteristic of quadcopters, to quantify the wind disturbance acting on the systems, as well as reflect the maneuverability of quadcopters, this paper employs simulation to quantify the uncertainty.

This paper proposes a two-step adaptive AirMatrix design procedure for adaptive AirMatrix, by separately calculating the block size affected by GPS signal quality and wind disturbance. The paper is organized as follows. Section II first introduces the definition of the adaptive AirMatrix structure, and then analyzes the factors that influence the model design. Section III provides a detailed design approach for adaptive AirMatrix, including the GPS-induced and wind-induced deviation models. Section IV discusses the safety and capacity performance of the proposed model. Section V concludes the findings of this research and discusses future work.

II. THE FUNDAMENTAL OF THE ADAPTIVE AIRMATRIX STRUCTURE

The block size of the AirMatrix structure should ensure the probability of the quadcopter appearing at the border within the safety tolerance P_{ST}. Hence, we defined the block size S_I of AirMatrix as (1), as is illustrated in Fig.2.

$$S_I = 2(R_{drone} + D_{ST}) \tag{1}$$

where, R_{drone} represents the farthest position of the quadcopter away from its geometric center. D_{ST} represents the acceptable track deviation under P_{ST}. The setting of P_{ST} can be guided by the Equivalent Level of Safety (ELOS), which is defined as the general safety objective for UAVs should be equivalent to civil aviation [34].

The block size is related to the acceptable track deviation of quadcopters. In this paper, GPS-induced deviation e_{GPS} and wind-induced deviation e_{wind} are the main considerations. The former has its probability distribution related to levels of GPS signal quality, which is introduced in Section III. The latter is an expansion of R_{drone} considering the wind effect as it can lead to the farthest position of quadcopters deviating from its origin (Fig.2). Then, the equivalent quadcopter size R'_{drone} under the wind impact can be defined as (2). In this way, under the wind impact, the corrected block size S_C can be expressed as (3).

$$R'_{drone} = R_{drone} + e_{wind} \tag{2}$$

$$S_C = S_I + 2e_{wind} \tag{3}$$

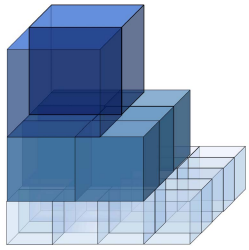

Fig. 3. Illustration of the adaptive AirMatrix model.

Two main factors should be noted when calculating the e_{wind}. First, surface friction and turbulence should be considered when building the wind impact model. Under the influence of surface friction, the horizontal wind speed accelerates with the distance from the ground. The quadcopter experiences intenser horizontal wind disturbance and deviates further from its track. Surface friction also leads to uneven atmosphere distribution in the low-altitude airspace, which makes the fluid movement in the canopy and boundary layer of urban a state of turbulence. The turbulence would influence the position of the quadcopter as well. Since the safety tolerance of collision rate is predefined and fixed, the block size on each layer of adaptive AirMatrix increases along with altitude considering the disturbance at high altitudes is more significant. Based on the analysis above, the sketch of the adaptive AirMatrix is shown in Fig.3.

Second, quadcopters are nonlinear and under-actuated systems, its dynamic should be considered when quantifying the wind effect. We assume the quadcopter is a rigid and symmetrical structure with constant mass and inertia, whose geometric center and the center of gravity coincides. The propellers are rigid, with the odd one rotating counterclockwise, and the even one rotating clockwise. We model the wind effect on the quadcopter as a drag force in the inertial frame [32]. North-East-Down (NED) and Forward-Right-Down (FRD) are used for the inertial frame and the body frame respectively. Hence, when the quadcopter is under gravity, wind impact, and thrust, the quadcopter dynamics in the inertial frame are given by [35]:

$$\begin{bmatrix} \dot{v}_x \\ \dot{v}_y \\ \dot{v}_z \\ \dot{\phi} \\ \dot{\theta} \\ \dot{\psi} \end{bmatrix} = \begin{bmatrix} -Tm^{-1}(\sin\psi\sin\phi+\cos\psi\sin\theta\cos\phi)+m^{-1}f_x \\ -Tm^{-1}(-\cos\psi\sin\phi+\sin\psi\sin\theta\cos\phi)+m^{-1}f_y \\ g - Tm^{-1}\cos\phi\cos\theta + m^{-1}f_z \\ p + q\sin\phi\tan\theta + r\cos\phi\tan\theta \\ q\cos\phi - r\sin\phi \\ q\sin\phi\cos\theta^{-1} + r\cos\phi\cos\theta^{-1} \end{bmatrix}, \tag{4}$$

where $\dot{v} = \left[\dot{v}_x, \dot{v}_y, \dot{v}_z\right]^{\mathrm{T}}$ is the linear acceleration of the center of mass; $\Theta = [\dot{\phi}, \dot{\theta}, \dot{\psi}]^{\mathrm{T}}$ refers to the change rate of the Euler angles. m is the total mass of the quadcopter, g is the standard local gravity, $f = \left[f_x, f_y, f_z\right]^{\mathrm{T}}$ refers to wind force components in each axis. $\Omega = [p, q, r]^{\mathrm{T}}$ refers to the angular velocity of the quadcopter within the body frame. T refers to the total thrust generated by propellers, which can be given by

$$T = \sum_{i=1}^{4} C_T \omega_i^2, \tag{5}$$

where C_T is the thrust coefficient, ω_i is the angular velocity of the rotor.

Based on the Euler equation, the angular acceleration $\dot{\Omega} = [\dot{p}, \dot{q}, \dot{r}]^{\mathrm{T}}$ is computed as

$$\begin{bmatrix} \dot{p} \\ \dot{q} \\ \dot{r} \end{bmatrix} = \begin{bmatrix} I_{xx}^{-1}[\tau_x + qr(I_{yy} - I_{zz}) - \tau_{dx} + J_{RP}q\bar{\omega}] \\ I_{yy}^{-1}[\tau_y + pr(I_{zz} - I_{xx}) - \tau_{dy} - J_{RP}p\bar{\omega}] \\ I_{zz}^{-1}[\tau_z + pq(I_{xx} - I_{yy}) - \tau_{dz}] \end{bmatrix}, \tag{6}$$

where $J = \mathrm{diag}[I_{xx}, I_{yy}, I_{zz}]$ is the inertia matrix of the quadcopter; J_{RP} represents the total moments of inertia of the entire rotor, and the propeller about the axis of rotation, $\overline{\omega} = \omega_1 - \omega_2 + \omega_3 - \omega_4$ refers to the sum of the rotor speed. $\tau = \left[\tau_x, \tau_y, \tau_z\right]^{\mathrm{T}}$ refer to moments generated by the propellers, which is related with quadcopter configuration, thrust coefficient, torque coefficient and rotor speed. $\tau_d = [\tau_{dx}, \tau_{dy}, \tau_{dz}]^{\mathrm{T}}$ is the aerodynamical friction moments, which is expressed by [32]:

$$\begin{bmatrix} \tau_{dx} \\ \tau_{dy} \\ \tau_{dz} \end{bmatrix} = \begin{bmatrix} k_{dx}p^2 \\ k_{dy}q^2 \\ k_{dz}r^2 \end{bmatrix} \tag{7}$$

where $k_d = \mathrm{diag}[k_{dx}, k_{dy}, k_{dz}]$ is friction moments coefficients along corresponding axis.

With the highly nonlinear and coupling characteristic, quadcopters depend on their control system to stabilize their attitude and achieve the desired trajectory. The proportional integral derivative (PID) algorithm is classical control law that is widely applied in quadcopter control systems due to its simplicity and practicability [24]. Therefore, to reflect the ability of quadcopters to maneuver in a wind field, we employed the PID-based quadcopter dynamic modeling and simulation system developed by Hartman et al. from the university of Drexel based on MATLAB Simulink [36] to calculate the wind-induced deviation. The system is named Quadcopter Dynamic Modeling and Simulation (Quad-Sim) v1.00. The wind impact model can be inputted into the External Disturbances module of Quad-Sim to assess the corresponding track deviation. The details of the calculation method of acceptable GPS-induced deviation and wind-induced deviation are introduced in Section III.

III. Methods to Calculate the Block Size in AirMatrix

This Section first introduces how to calculate acceptable GPS-induced and wind-induced deviation in corresponding environments. Then, the design procedure of the adaptive AirMatrix model is provided.

A. GPS-Induced Deviation

Position uncertainty of quadcopter can be modeled using approximated probabilistic methods [37]. Based on the experiments support [18] and considering the repeatability and similarity of the random error in the navigation system, we assume

TABLE II
POSITION DEVIATION OF QUADCOPTERS UNDER UNIFORM DISTRIBUTION SIGNAL PATTERNS

Density	Latitude		Longitude	
	Mean (m)	Standard Dev. (m)	Mean (m)	Standard Dev. (m)
1	1.51	1.34	1.61	1.26
0.7	1.63	1.35	1.86	1.38
0.5	1.69	1.58	1.86	1.37
0.3	1.69	1.75	2.12	1.61
0.1	2.39	2.67	2.67	1.99
0.05	3.34	3.64	2.73	2.12
0.03	5.86	4.84	4.68	3.36
0.02	9.75	5.25	8.12	5.46
0.01	13.53	7.19	11.30	7.87

TABLE III
POSITION DEVIATION OF QUADCOPTERS UNDER NON-UNIFORM DISTRIBUTION SIGNAL PATTERNS

Distribution	Latitude		Longitude	
	Mean (m)	Standard Dev. (m)	Mean (m)	Standard Dev. (m)
Gaussian	5.99	3.85	6.80	5.80
Sin	5.99	3.90	4.33	3.82
Random	5.80	3.92	4.33	3.89

the GPS-induced deviation of the quadcopter in each direction follows the Gaussian distribution, which can be given by

$$e_{GPS-axis} \sim N(0, \sigma_{GPS}^2), \tag{8}$$

where, $e_{GPS-axis}$ represents the GPS-induced position deviation on the axis x, y, z. σ_{GPS} is the standard deviation of the position deviation influenced by the GPS signal quality. Given independent and isotropic GPS accuracies, we assume σ_{GPS} is related with GPS signal quality and equivalent in three directions.

To simplify the calculation, under the distribution of e_{GPS}, acceptable GPS-induced deviation D_{ST} is given by (9), which represents that the probability of the quadcopter appearing at the border should meet the safety tolerance P_{ST}.

$$P(x = D_{ST}, y = 0, z = 0) = P_{ST}. \tag{9}$$

GPS signal data show different distribution patterns in different environments [38]. In specific, when the satellite link is unstable, the signal data normally shows a uniform distribution. When there is an extreme atmosphere or physical interference, signal data normally shows Gaussian distribution, Sin distribution, and Random distribution [39]. Pang et al. [38] employed the Extended Kalman Filter (EKF) algorithm to access the track deviation distribution of UAVs under different GPS signal patterns, which can guide the acceptable distance thresholds setting for UAVs under corresponding signal environments. Table II and Table III record the mean and standard deviation of GPS-induced deviation under signal patterns with uniform distribution and non-uniform distribution respectively. To supplement the data of position deviation under signal with uniform distribution, we employ the curve fitting tool in MATLAB to fit the function of signal density ρ_{GPS} vs. position deviation σ_{GPS}. The worse standard deviation in two directions for each signal density is chosen as σ_{GPS} to accomplish the fitting. The function is given by

$$\sigma_{GPS} = 0.57 + \rho_{GPS}^{-0.55} + 0.71. \tag{10}$$

TABLE IV
GOODNESS OF FITTING RESULTS

	SSE	R-square	Adjusted R-square	RMSE
Value	0.08027	0.9981	0.9974	0.1157

The goodness of fitting results is recorded in Table IV. The R-squared and Adj R-square are close to 1. The Sum of the Squared Errors (SSE) and Root Mean Squared Error (RMSE) also demonstrate the goodness of fitting.

B. Wind-Induced Deviation

The wind effect model acting on quadcopter is modeled as a force in the inertial frame. According to the formula of air resistance [40], the wind impact on quadcopter can be denoted as

$$f_{axis} = \frac{1}{2}\rho c_{axis} s_{axis} v_{axis}^2, \tag{11}$$

where, f_{axis} represents the wind force component in corresponding axis, c_{axis} is the drag coefficient along the corresponding axis, v_{axis} represents the relative wind speed component on each axis, ρ is the air density and s_{axis} is the projected area seen by the wind in each direction.

As is analyzed in the Section II, surface friction and turbulence effects should be considered. Hence, the wind model can be divided into a dominant wind model and a turbulence model. The details are introduced in the following.

C. Dominant Wind Model

The dominant wind, which is also called static wind, can be obtained by the largest wind speed and direction in meteorological estimation.

Under the influence of surface friction, the wind speed closes to the surface will decrease. The flow of the atmosphere will not be affected by the surface after reaching the gradient height [41]. This kind of distribution of wind speed along the height is called wind speed profile and can be denoted as power law, as expressed by (12).

$$V(z) = V_R \left(\frac{z}{z_R}\right)^a \tag{12}$$

where, $V(z)$ represents the average wind speed at height z. V_R is the reference wind speed at the reference height. a refers to the ground roughness coefficient, which is affected by terrain, stratification stability, and other factors.

According to the American Society of Civil Engineers [42], in the urban environment, a and gradient height have values of 0.4 and 450m, respectively. Hence, the wind speed profile below the gradient height can be expressed as

$$V(z) = V_R \left(\frac{z}{10}\right)^{0.4}. \tag{13}$$

D. Turbulence Model

Turbulence is a stochastic process that velocity spectra can express. Dryden and von Karman models are classic models employed in simulating turbulence in evaluating aircraft performance [43]. According to the Military Specification MIL-F-8785C [44], the horizontal and vertical components of the power spectra density function for turbulence are expressed as follows.

$$\Phi_h(\Omega) = \frac{\sigma_h^2 2L_h}{\pi} \cdot \frac{1}{1+(L_h\Omega)^2} \tag{14}$$

$$\Phi_v(\Omega) = \frac{\sigma_v^2 L_v}{\pi} \cdot \frac{1+3\,(L_v\Omega)^2}{\left[1+(L_v\Omega)^2\right]^2} \tag{15}$$

where, Ω represents the selected frequency, L_h and L_v represents the turbulence scale length, σ_h and σ_v represents the turbulence intensity. According to the MIL-F-8785C [43], below 1000ft, the length scale and turbulence intensity of vertical component can be expressed as $L_v = h$, $\sigma_v = 0.1W_{20}$. h refers to the flight height. W_{20} represents the wind speed at 20 feet. Typically, W_{20} is 15 knots (7.5 m/s) in light turbulence, 30 knots (15m/s) in moderate turbulence, and 45 knots (22.5m/s) in severe turbulence. Then, the length scale and turbulence intensity of the horizontal component of turbulence can be obtained by the follows.

$$L_h = \frac{L_v}{(0.177+0.000823h)^{1.2}} \tag{16}$$

$$\sigma_h = \frac{\sigma_v}{(0.177+0.000823h)^{0.4}} \tag{17}$$

According to the Large-Eddy simulation in an urban environment [45], the standard deviation of turbulence intensity and pulse velocity in the urban canopy and boundary layer is relatively small. Hence, in this paper, the turbulence scale length is regarded as fixed.

E. Design Procedure of Adaptive AirMatrix Model

The sizes of quadcopters operating in one specific airspace will be slightly different. To meet the safety requirement of all the quadcopters, R_{drone} is determined by the largest quadcopter in one specific airspace when calculating the initial block size S_I. When calculating the corrected block size S_C, the wind induced deviation e_{wind} is determined by the quadcopter most susceptible to disturbance (the largest e_{wind}).

The adaptive AirMatrix model design procedure is shown in Fig.4. The block size on each layer is calculated recursively based on the inputted parameters, until reaching the upper border of the airspace.

In detail, on Layer one, the initial block size S_I is determined by R_{drone} and D_{ST}. D_{ST} is obtained by the acceptable deviation of the quadcopter under the corresponding GPS signal quality. Then, to calculate the corrected block size, the turbulence induced deviation e_t will be first calculated by employing the Quad-Sim. The height of the Layer one H_1 then can be obtained by (18). Subsequently, the horizontal wind speed on H_1 can be obtained. Wind induced deviation at H_1 can be assessed by employing the Quad-Sim. After that, the corrected block size one Layer one S_{C-1} can be updated based on (19), where e_{wind} represents the largest deviation in three directions.

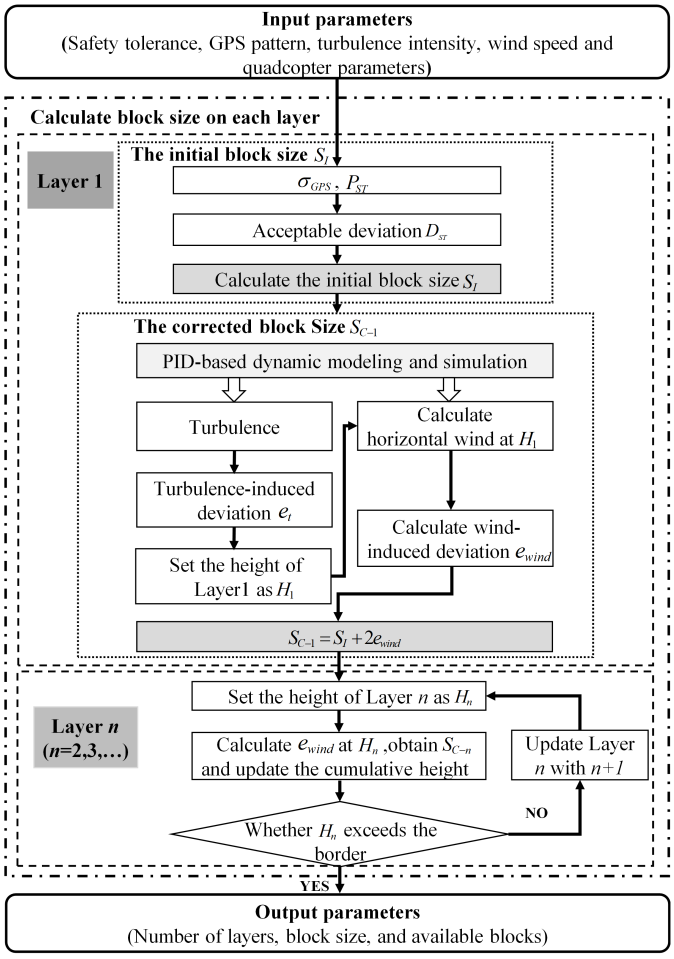

Fig. 4. Design procedure of the adaptive AirMatrix model.

$$H_1 = S_I + 2e_t \tag{18}$$

$$S_{C-n} = S_I + 2e_{wind} \tag{19}$$

Subsequently, layer number increases by one. For the Layer n ($n = 2, 3, \ldots$), update their heights H_n as follow.

$$H_n = \sum_{i=2}^{n} S_{C-(i-1)} + S_{C-(n-1)} \tag{20}$$

The corrected block size of Layer n is obtained based on (19) after calculating e_{wind} on H_n. The block size will be calculated recursively for each layer until cumulative height exceeds the upper border of the airspace.

A contingency management module will be activated when communication dropouts or other emergency scenarios happen Once the contingency management module is activated, the S_I of airspace will be designed based on the worst GPS signal pattern. In this paper, the worst GPS signal quality pattern in [38] is employed, with its σ_{GPS} having a value of 7.0m.

IV. Results and Discussion

The above procedure allows us to design dynamic airspace for quadcopters in different GPS signal quality and wind

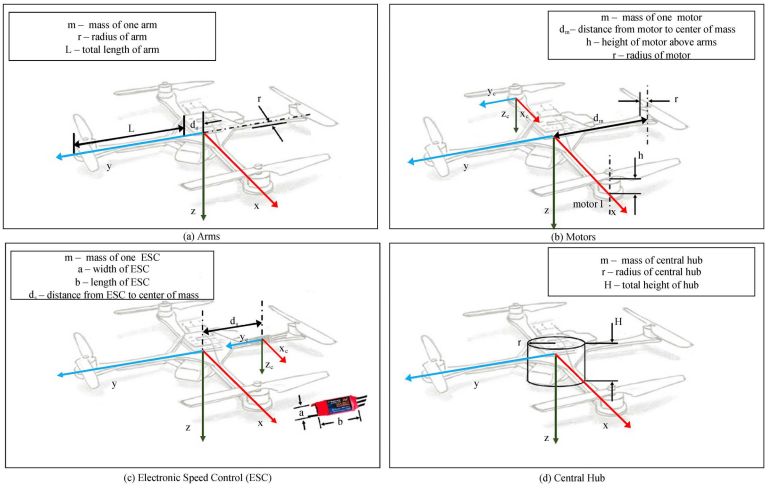

Fig. 5. Illustration of the main components of the Quadcopter1.

TABLE V
PARAMETERS OF PID CONTROL

Roll			Pitch			Yaw			Altitude		
Kp	Ki	Kd	Kp	Ki	Kd	Kp	Ki	Kd	Kp	Ki	Kd
2	1.1	1.2	2	1.1	1.2	4	0.5	3.5	2	1.1	3.3

TABLE VI
PARAMETERS OF TWO TYPES OF QUADCOPTERS IN SCENARIO

Quadcopter	Weight (g)	R_{drone} (mm)
1	1023	240
2	1480	250

environments. In this Section, we study the scalability of the Adaptive AirMatrix in different environments. Then, we compare the capacity and safety performance of the Adaptive AirMatrix model with other airspace models.

A. Scenario of Model Validation

In the scenario of model validation, two types of plus (+) structure quadcopters are equipped with the same controller system, but with different weights and sizes. Their PID controller parameters that are responsible for roll control, yaw control, pitch control, and altitude control are recorded in Table V. Their weight and size parameters are recorded in Table VI. In general, Quadcopter2 has the larger R_{drone} and weight, but Quadcopter1 is lighter and more susceptible to disturbance. Hence, the initial block size is determined by the Quadcopter2, and the corrected block size is determined by the wind-induced deviation of Quadcopter1.

The structure and main components of the Quadcopter1 are illustrated in Fig.5. Its components and system parameters are recorded in Table VII and Table VIII. The structure and the size of Quadcopter1 are similar with the quadcopter designed by Faessler et al. [46]. Based on it, the drag coefficient of Quadcopter1 is set as 0.2.

B. Initial Block Sizes Under Different GPS Signal Patterns

First, we calculated the initial block size S_I of adaptive AirMatrix under different GPS signal quality when P_{ST} is chosen as 1×10^{-8}. The initial block sizes under different GPS signal patterns are recorded in Table IX.

The results show that, when the GPS data shows the uniform distribution, the initial block size increases exponentially with the decrease of GPS density. The S_I of AirMatrix will be very large when GPS data shows non-uniform distribution, which is about four times larger than that in good signal quality.

Especially, when the communication dropouts and other emergency situations happen, the contingency management pattern will be activated. Under the pre-defined safety tolerance 1×10^{-8}, S_I is set as 70.10m.

C. Capacity Performance of Adaptive AirMatrix Model

Then, we verify the capacity performance of the adaptive AirMatrix model. A similar scenario with [18] is adopted. The size of the airspace is $2000m \times 2000m \times 200m$. The GPS shows uniform distribution with a density of 0.9 and P_{ST} is set as 1×10^{-8}. Hence, the S_I is 15m. The turbulence intensity is set as moderate and horizontal wind comes from the x axis of the quadcopter with a reference speed of 5.4m/s. The capacity perfromance of Dai's model [18] and Pongsakornsathien's model [17] are recorded in Table X. Since these airspace models did not consider the wind impact, their block sizes do not change under wind disturbance.

Fig.6 illustrates the layers structures in three airspace model. In general, the capacity of adaptive AirMatrix is the best since it maximizes the efficiency of airspace resource exploitation. The Dai's model only contains 5 layers and 12500 blocks due to the overset of block size. The number of the available blocks in Pongsakornsathiel's model is between the former two models, 31.2% less than that of the adaptive AirMatrix but 11 times more than that of the Dai's model. The adaptive AirMatrix divides the airspace into 13 layers, which is the most in three models.

Fig.7 shows the available blocks of different models under different altitudes. In general, the available blocks number of the adaptive AirMatrix model is relatively more in all the scenarios, showing its superior in capacity performance. The performance of Dai's model is worst among all the

TABLE VII
COMPONENTS PARAMETERS OF QUADCOPTER1

Arm		Motor		Electronic Speed Control (ESC)		Central Hub	
Parameters	Value	Parameters	Value	Parameters	Value	Parameters	Value
weight	45g	weight	73g	weight	30g	weight	431g
radius	33mm	distance to center	202mm	length	58mm	radius	57mm
length	170mm	height	32mm	width	26mm	height	43mm
distance to center	41mm	radius	140mm	distance to center	83mm		

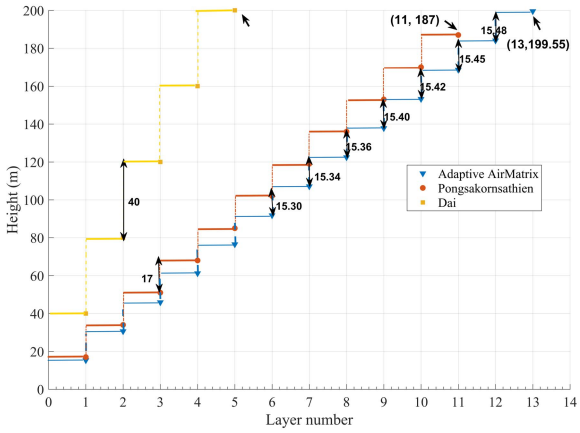

Fig. 6. Comparison of layers structures in different airspace models.

TABLE VIII
RELATED PARAMETERS OF QUADCOPTER1

Parameters	Values
J (kg · m^2)	$\mathrm{diag}\left[9.5, 9.5, 18.4\right]^{\mathrm{T}} \times 10^{-3}$
J_{RP} (kg · m^2)	1.25×10^{-5}
k_d (kg · m)	$\mathrm{diag}\left[5.57, 5.57, 6.35\right]^{\mathrm{T}} \times 10^{-4}$
C_T (kg · m)	1.49×10^{-7}

scenarios since the block size setting is too large. When the upper border of airspace is set as 200 meters, the adaptive AirMatrix has more 45 percentage of available blocks than that in Pongsakornsathien's model. The number of available blocks in the adaptive AirMatrix and Pongsakornsathien's are approximately equal below 100 meters. In this scenario, the utilization rate of the airspace in adaptive AirMatrix is poor and much of the airspace is wasted.

D. Safety Performance of Adaptive AirMatrix

The safety improvement of adaptive AirMatrix model mainly reflects in two aspects. First, the adaptive AirMatrix model considers the wind impact on track accuracy which is not considered in other models. Second, a PID-based quadcopter dynamic model and simulation system is employed to assess the wind-induced deviation, which reflect the dynamics of quadcopter and makes the design more precise.

Table XI and Table XII record S_{C-1} under different horizontal wind speeds and turbulence intensity. The wind comes from the x-axis of the quadcopter and S_I is set as 20.50m. The safety improvement refers to the effectiveness of corrected block sizes in ensuring the safety target. The results show that along with the increase in disturbance, the effectiveness of corrected block in improving safety becomes more obvious.

In addition, the better the GPS signal quality is, the more essential the corrected block size in ensuring airspace safety. Fig.8 shows the safety improvement of the corrected blocks under different GPS signal patterns. Under the same wind impact, the wind-induced corrected block size has a higher safety improvement rate when the GPS signal quality is better.

TABLE IX
INITIAL BLOCK SIZE UNDER DIFFERENT GPS SIGNAL PATTERNS

Signal Pattern	σ_{GPS} (m)	Initial Block Size S_I (m)
1	1.28	14.90
0.90	1.30	15.00
0.70	1.40	16.20
0.50	1.54	17.70
0.30	1.82	20.50
0.10	2.73	29.90
Gaussian	5.80	59.70
Sine	3.90	41.50
Random	3.92	41.70
Contingency	7.00	70.10

TABLE X
CAPACITY PERFORMANCE OF THE PREVIOUS AIRMATRIX MODELS

Source	Block size (m)	Layers	Available blocks
[18]	40	5	12500
[17]	17	11	150579

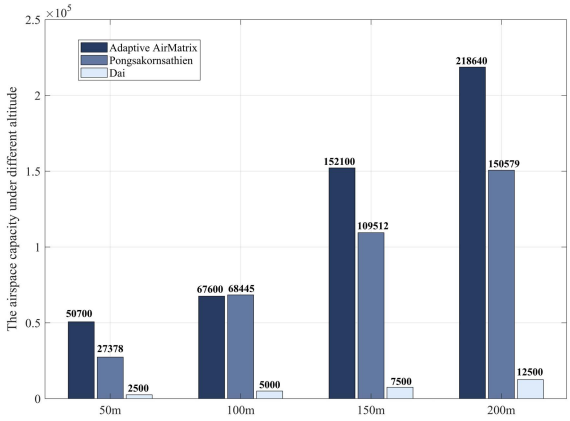

Fig. 7. Comparison of airspace capacity under different altitudes.

TABLE XI
CORRECTED BLOCK SIZE UNDER DIFFERENT HORIZONTAL WIND SPEED

Wind speed (m/s)	S_{C-1} (m)	Safety improvement (%)
5.4	20.55	12.1
7.9	20.60	22.0
8.4	20.61	22.3
10.3	20.67	31.1
12.3	20.74	38.5
13.6	20.79	51.3
15.1	20.86	56.7
16.6	20.93	61.6

TABLE XII
CORRECTED BLOCK SIZE UNDER DIFFERENT TURBULENCE INTENSITY

	S_{C-1} (m)	Safety improvement (%)
Light turbulence	20.56	4.9
Moderate turbulence	20.80	49.7
Severe turbulence	21.92	95.5

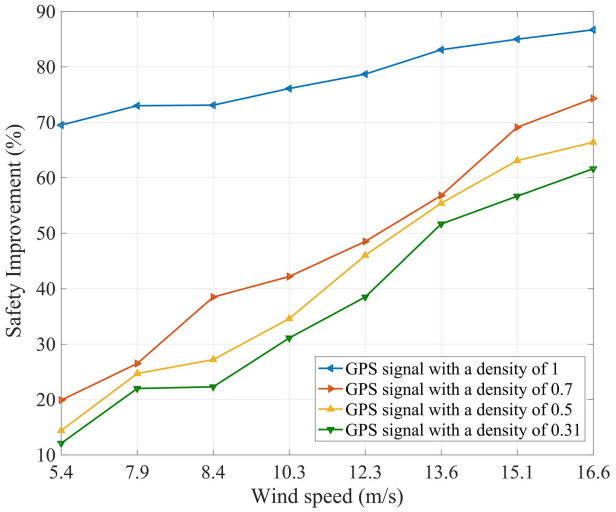

Fig. 8. Safety improvement of the corrected blocks under different GPS signal patterns and wind environments.

E. Effectiveness of Quad-Sim

The effectiveness of Quad-Sim applied in accessing wind induced deviation reflects in two aspects. For one thing, Quad-Sim can reflect the dynamics of quadcopters. Fig.9 illustrates the vertical position performance of the quadcopter under different disturbance when it is targeted at hovering. The light blue line illustrates the vertical position of the aircraft with 1 N disturbance from the x-axis while the dark blue line illustrates the vertical position of aircraft in a non-disturbed environment. The results show that even though there is no external disturbance or with disturbance comes from the x-axis, the vertical position of the quadcopter will deviate from its target. This phenomenon attributes to the reason that quadcopter is an underactuated and coupling system that needs change pitch, yaw, and roll angle to maintain its altitude when overcome the gravity or subjected to external disturbance.

For another thing, compared with the method of regarding disturbances as vectors, Quad-Sim can better reflect the position response and effect of controller. Beaufort wind force

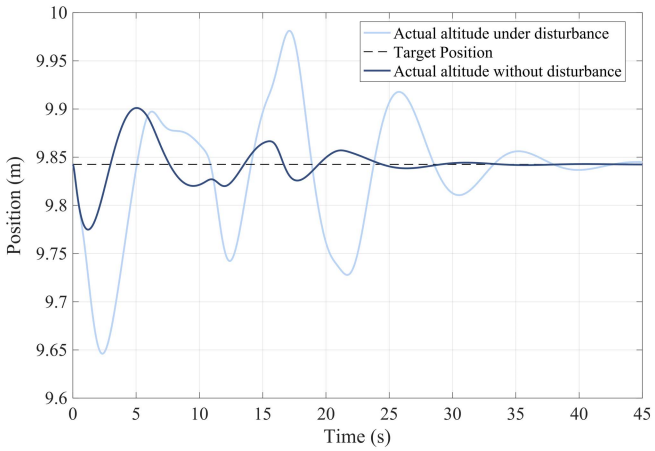

Fig. 9. Comparison of vertical position response in different environments.

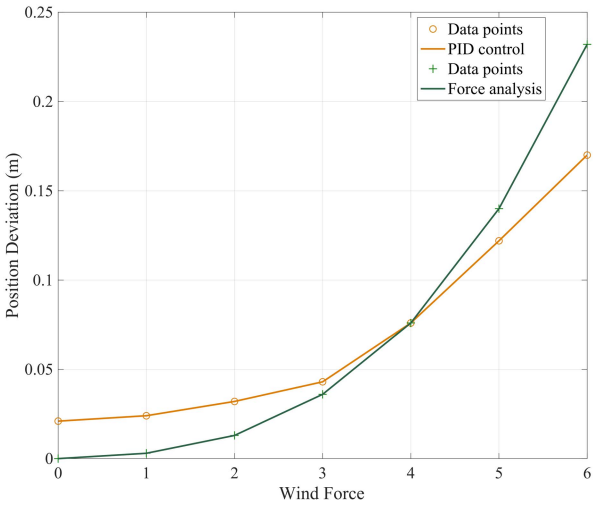

Fig. 10. Comparison of wind-induced deviation under different calculation methods.

scale is an international metric for wind classification, and we take the maximum wind speed on each level to calculate the wind impact. Fig.10 illustrates the wind-induced position deviation of the quadcopter calculated by the Quad-Sim and force analysis respectively. When the wind force is light (0-3), the deviation calculated based on the Quad-Sim is more significant than that calculated by force analysis. It illustrates that Quad-Sim can better reflect the position response of the quadcopter under gentle disturbance. In this way, Quad-Sim can ensure a safer corrected block. Meanwhile, when the wind is strong (5-6), the deviation calculated based on the Quad-Sim is less than that of the force analysis, which reflects the effect of the controller on eliminating disturbance. In this situation, the corrected block size calculated by Quad-Sim can better guarantee the utilization of airspace. Therefore, the corrected block designed by employing the Quad-Sim is more accurate.

V. CONCLUSION

This paper proposed an adaptive AirMatrix model for quadcopters in Urban Air Mobility, which helps manage the collision risk among quadcopters under different GPS

signal quality and wind environments. The dynamics and control characteristics of the quadcopters are considered in designing the AirMatrix. The results show that the proposed AirMatrix model can reduce the conserveness of airspace design. Moreover, by considering the wind-induced deviation, the corresponding block setting can better manage collision probability and ensure the safety target.

System models and system theory can access the overall uncertainty of quadcopter in a more theoretical and reliable way. Ongoing research efforts are addressing quantifying the coupling mechanism of different disturbances acting on the quadcopters, modeling both parametric and nonparametric uncertainty in the system model, thus designing the airspace model for quadcopters based on reachable set computation. Moreover, in the future, after practical application of the AirMatrix and getting massive UAVs traffic data, the reliability of the adaptive AirMatrix design can be further evaluated by REICH collision risk model and its improved models.

REFERENCES

[1] H. Shakhatreh et al., "Unmanned aerial vehicles (UAVs): A survey on civil applications and key research challenges," *IEEE Access*, vol. 7, pp. 48572–48634, 2019, doi: 10.1109/ACCESS.2019.2909530.

[2] H. Tang, Y. Zhang, V. Mohmoodian, and H. Charkhgard, "Automated flight planning of high-density urban air mobility," *Transp. Res. C, Emerg. Technol.*, vol. 131, pp. 103324–103343, Oct. 2021, doi: 10.1016/j.trc.2021.103324.

[3] Z. Wu and Y. Zhang, "Integrated network design and demand forecast for on-demand urban air mobility," *Engineering*, vol. 7, no. 4, pp. 473–487, Apr. 2021, doi: 10.1016/j.eng.2020.11.007.

[4] K. P. Valavanis and G. J. Vachtsevanos, *Handbook of Unmanned Aerial Vehicles*. Berlin, Germany: Springer, 2015.

[5] J. Bertram and P. Wei, "Distributed computational guidance for high-density urban air mobility with cooperative and non-cooperative collision avoidance," in *Proc. AIAA Scitech Forum*, Jan. 2020, pp. 1371–1384.

[6] E. Sunil et al., "Metropolis: Relating airspace structure and capacity for extreme traffic densities," in *Proc. USA/Eur. Air Traffic Manag. Res. Dev. Semin. (ATM)*, Lisboa, Portuga, 2015, pp. 1–11.

[7] C. Ramee and D. N. Mavris, "Development of a framework to compare low-altitude unmanned air traffic management systems," in *Proc. AIAA Scitech Forum*, Jan. 2021, pp. 1–24.

[8] J. M. Hoekstra, R. N. Van Gent, and R. C. Ruigrok, "Designing for safety: The 'free flight' air traffic management concept," *Reliab. Eng. Syst. Safe.*, vol. 75, no. 2, pp. 215–232, Feb. 2002, doi: 10.1016/S0951-8320(01)00096-5.

[9] T. Prevot, V. Battiste, E. Palmer, and S. Shelden, "Air traffic concept utilizing 4D trajectories and airborne separation assistance," in *Proc. AIAA Guid., Navigat., Control Conf. Exhibit*, Austin, TX, USA, Aug. 2003, p. 5770.

[10] E. Sunil, J. Ellerbroek, J. M. Hoekstra, and J. Maas, "Three-dimensional conflict count models for unstructured and layered airspace designs," *Transp. Res. C, Emerg. Technol.*, vol. 95, pp. 295–319, Oct. 2018, doi: 10.1016/j.trc.2018.05.031.

[11] E. Sunil et al., "The influence of traffic structure on airspace capacity," in *Proc. 7th Int. Conf. Res. Air Transp. (ICRAT)*, Ann Arbor, MI, USA, 2016, pp. 1–9.

[12] X. Zhang, Y. Liu, Y. Zhang, X. Guan, D. Delahaye, and L. Tang, "Safety assessment and risk estimation for unmanned aerial vehicles operating in national airspace system," *J. Adv. Transp.*, vol. 2018, pp. 1–11, Oct. 2018, doi: 10.1155/2018/4731585.

[13] X. Hu, B. Pang, F. Dai, and K. H. Low, "Risk assessment model for UAV cost-effective path planning in urban environments," *IEEE Access*, vol. 8, pp. 150162–150173, 2020, doi: 10.1109/ACCESS.2020.3016118.

[14] Y. Wu and K. H. Low, "An adaptive path replanning method for coordinated operations of drone in dynamic urban environments," *IEEE Syst. J.*, vol. 15, no. 3, pp. 4600–4611, Sep. 2021, doi: 10.1109/jsyst.2020.3017677.

[15] B. Pang, W. Dai, T. Ra, and K. H. Low, "A concept of airspace configuration and operational rules for UAS in current airspace," in *Proc. AIAA/IEEE 39th Digit. Avionics Syst. Conf. (DASC)*, Antonio, TX, USA, Oct. 2020, pp. 1–9.

[16] M. F. B. M. Salleh et al., "Preliminary concept of adaptive urban airspace management for unmanned aircraft operations," in *Proc. AIAA Infotech Aerosp.*, Kissimmee, FL, USA, 2018, pp. 1–12.

[17] N. Pongsakornsathien, S. Bijjahalli, A. Gardi, R. Sabatini, and T. Kistan, "A novel navigation performance-based airspace model for urban air mobility," in *Proc. AIAA/IEEE 39th Digit. Avionics Syst. Conf. (DASC)*, San Antonio, TX, USA, Oct. 2020, pp. 1–6.

[18] W. Dai, B. Z. Pang, and K. H. Low, "Conflict-free four-dimensional path planning for urban air mobility considering airspace occupancy," *Aerosp. Sci. Technol.*, vol. 119, pp. 107154–107170, Dec. 2021, doi: 10.1016/j.ast.2021.107154.

[19] Y. Wu, K. H. Low, B. Pang, and Q. Tan, "Swarm-based 4D path planning for drone operations in urban environments," *IEEE Trans. Veh. Technol.*, vol. 70, no. 8, pp. 7464–7479, Aug. 2021, doi: 10.1109/TVT.2021.3093318.

[20] Y. Wu, K. H. Low, and X. Hu, "Trajectory-based flight scheduling for AirMetro in urban environments by conflict resolution," *Transp. Res. C, Emerg. Technol.*, vol. 131, pp. 103355–103376, Sep. 2021, doi: 10.1016/j.trc.2021.103355.

[21] Y. Wu and K. H. Low, "Discrete space-based route planning for rotary-wing UAV formation in urban environments," *ISA Trans.*, vol. 129, pp. 243–259, Oct. 2022, doi: 10.1016/j.isatra.2021.12.043.

[22] Y. Wu, S. Wu, and X. Hu, "Cooperative path planning of UAVs & UGVs for a persistent surveillance task in urban environments," *IEEE Internet Things J.*, vol. 8, no. 6, pp. 4906–4919, Mar. 2021, doi: 10.1109/JIOT.2020.3030240.

[23] N. Zhang, M. C. Zhang, and K. H. Low, "3D path planning and real-time collision resolution of multirotor drone operations in complex urban low-altitude airspace," *Transp. Res. C, Emerg. Technol.*, vol. 129, pp. 103123–103146, Aug. 2021, doi: 10.1016/j.trc.2021.103123.

[24] B. J. Emran and H. Najjaran, "A review of quadrotor: An underactuated mechanical system," *Annu. Rev. Control*, vol. 46, pp. 165–180, Jan. 2018, doi: 10.1016/j.arcontrol.2018.10.009.

[25] C. Llanes, M. Abate, and S. Coogan, "Safety from fast, in-the-loop reachability with application to UAVs," in *Proc. ACM/IEEE 13th Int. Conf. Cyber-Phys. Syst. (ICCPS)*, May 2022, pp. 127–136, doi: 10.1109/ICCPS54341.2022.00018.

[26] S. Coogan, "Mixed monotonicity for reachability and safety in dynamical systems," in *Proc. 59th IEEE Conf. Decis. Control (CDC)*, Dec. 2020, pp. 5074–5085, doi: 10.1109/CDC42340.2020.9304391.

[27] M. Abate, M. Dutreix, and S. Coogan, "Tight decomposition functions for continuous-time mixed-monotone systems with disturbances," *IEEE Control Syst. Lett.*, vol. 5, no. 1, pp. 139–144, Jan. 2021, doi: 10.1109/LCSYS.2020.3001085.

[28] S. Bak, T. T. Johnson, M. Caccamo, and L. Sha, "Real-time reachability for verified simplex design," in *Proc. IEEE Real-Time Syst. Symp.*, Dec. 2014, pp. 138–148, doi: 10.1109/RTSS.2014.21.

[29] Y. Lin and S. Saripalli, "Sampling-based path planning for UAV collision avoidance," *IEEE Trans. Intell. Transp. Syst.*, vol. 18, no. 11, pp. 3179–3192, Apr. 2017, doi: 10.1109/TITS.2017.2673778.

[30] N. K. Tran, E. Bulka, and M. Nahon, "Quadrotor control in a wind field," in *Proc. Int. Conf. Unmanned Aircr. Syst. (ICUAS)*, Denver, CO, USA, Jun. 2015, pp. 320–328.

[31] S. Waslander and C. Wang, "Wind disturbance estimation and rejection for quadrotor position control," in *Proc. AIAA*, Apr. 2009, pp. 1983–1996, doi: 10.2514/6.2009-1983.

[32] K. Eliker, S. Grouni, M. Tadjine, and W. Zhang, "Quadcopter nonsingular finite-time adaptive robust saturated command-filtered control system under the presence of uncertainties and input saturation," *Nonlinear Dyn.*, vol. 104, no. 2, pp. 1363–1387, Apr. 2021, doi: 10.1007/s11071-021-06332-3.

[33] A. Aboudonia, A. El-Badawy, and R. Rashad, "Active anti-disturbance control of a quadrotor unmanned aerial vehicle using the command-filtering backstepping approach," *Nonlinear Dyn.*, vol. 90, no. 1, pp. 581–597, 2017, doi: 10.1007/s11071-017-3683-y.

[34] R. A. Clothier and R. A. Walker, "Determination and evaluation of UAV safety objectives," in *Proc. 21st Int. Unmanned Air Veh. Syst. Conf.*, Bristol, U.K., 2006, pp. 18.1–18.16.

[35] Q. Quan, *Introduction to Multicopter Design and Control*. Berlin, Germany: Springer, 2017.

[36] D. Hartman, K. Landis, M. Mehrer, S. Moreno, and J. Kim. (2014). *Quadcopter Dynamic Modeling and Simulation (Quad-Sim) V1.00*. [Online]. Available: https://github.com/dch33/Quad-Sim
[37] S. Thrun, *Probabilistic Robotics*. Cambridge, MA, USA: MIT Press, 2005.
[38] B. Pang, E. M. Ng, and K. H. Low, "UAV trajectory estimation and deviation analysis for contingency management in urban environments," in *Proc. AIAA Aviation Forum*, Orlando, FL, USA, Jun. 2020, pp. 1–10.
[39] P. Huang and Y. Pi, "Urban environment solutions to GPS signal near-far effect," *IEEE Aerosp. Electron. Syst. Mag.*, vol. 26, no. 5, pp. 18–27, May 2011, doi: 10.1109/MAES.2011.5871387.
[40] F. B. Sorbelli, F. Coro, S. K. Das, and C. M. Pinotti, "Energy-constrained delivery of goods with drones under varying wind conditions," *IEEE Trans. Intell. Transp. Syst.*, vol. 22, no. 9, pp. 6048–6060, Sep. 2021, doi: 10.1109/TITS.2020.3044420.
[41] H. W. Tieleman, "Strong wind observations in the atmospheric surface layer," *J. Wind Eng. Ind. Aerodyn.*, vol. 96, no. 1, pp. 41–77, 2008, doi: 10.1016/j.jweia.2007.03.003.
[42] *Minimum Design Loads for Buildings and Other Structures*, ASCE, Standard ASCE/SEI 7, 2010, doi: 10.1061/9780784412916.
[43] T. R. Beal, "Digital simulation of atmospheric turbulence for Dryden and von Karman models," *J. Guid., Control, Dyn.*, vol. 16, no. 1, pp. 132–138, Jan. 1993, doi: 10.2514/3.11437.
[44] *Military Specification Flying Qualities of Piloted Airplanes, U.S. Military*, Standard MIL-F-8785C, 1980.
[45] W.-C. Cheng and F. Porté-Agel, "Adjustment of turbulent boundary-layer flow to idealized urban surfaces: A large-eddy simulation study," *Boundary-Layer Meteorol.*, vol. 155, no. 2, pp. 249–270, May 2015, doi: 10.1007/s10546-015-0004-1.
[46] M. Faessler, A. Franchi, and D. Scaramuzza, "Differential flatness of quadrotor dynamics subject to rotor drag for accurate tracking of high-speed trajectories," *IEEE Robot. Autom. Lett.*, vol. 3, no. 2, pp. 620–626, Apr. 2018, doi: 10.1109/LRA.2017.2776353.

Quan Shao was born in Ezhou, China, in 1981. He received the B.S. and M.S. degrees from the University of Science and Technology of China and the Ph.D. degree from the Institute of Public Safety, Tsinghua University, Beijing, China, in 2009. He is currently the Vice President, as well as a Professor with the College of Civil Aviation, Nanjing University of Aeronautics and Astronautics. His research interests include civil aviation safety management and emergency decision-making in civil aviation.

Ruoheng Li was born in Xuzhou, China, in 1998. She received the B.S. degree in engineering from the Nanjing University of Aeronautics and Astronautics, Nanjing, China, in 2020, and the B.S. degree in applied science (aviation) from the Royal Melbourne Institute of Technology University, Melbourne, VIC, Australia, in 2020. She is currently pursuing the M.S. degree in engineering with the Nanjing University of Aeronautics and Astronautics. Her current research interests include risk management of unmanned aircraft systems (UAS), UAS traffic management (UTM), and path planning algorithm of UAS.

Min Dong was born in Yancheng, China, in 1996. She received the B.S. degree in airport management from the Nanjing University of Aeronautics and Astronautics, Nanjing, China, in 2019, the B.S. degree in the applied science of aviation from the Royal Melbourne Institute of Technology University, Melbourne, VIC, Australia, in 2019, and the M.S. degree in transportation with the Nanjing University of Aeronautics and Astronautics. She is currently with the Department of system Technologies of Magnet Resonance Business Unit, United Imaging. Her current research interests include human factors and the safety management of civil aviation.

Chengcheng Song was born in Xinyang, China, in 1996. He received the B.S. degree in civil engineering from Hunan University, Changsha, China, in 2018, and the M.S. degree in transportation from the Nanjing University of Aeronautics and Astronautics. He is currently pursuing the Ph.D. degree in building energy modeling with Hunan University. His current research interests include evacuation, building energy, and computer vision.